Journal of Cleaner Production 242 (2020) 118444

Contents lists available at ScienceDirect

Journal of Cleaner Production

journal homepage: www.elsevier.com/locate/jclepro

Graphene-based thermionic-thermoradiative solar cells: Concept, efficiency limit, and optimum design

Xin Zhang [a, b], Yee Sin Ang [b], Jian-Ying Du [a], Jincan Chen [a, *], Lay Kee Ang [b, **]

[a] Fujian Key Laboratory of Semiconductors and Applications, Collaborative Innovation Center for Optoelectronic Semiconductors and Efficient Devices, And Department of Physics, Xiamen University, Xiamen, 361005, China
[b] Science and Math Cluster & Massachusetts Institute of Technology-International Design Center (SUTD-MIT IDC), Singapore University of Technology and Design, 8 Somapah Road, Singapore

ARTICLE INFO

Article history:
Received 18 June 2019
Received in revised form
27 August 2019
Accepted 15 September 2019
Available online 17 September 2019

Handling editor: Panos Seferlis.

Keywords:
Optoelectronic device
Thermionic emission
Thermoradiative conversion
Optimum operation

ABSTRACT

Solar energy conversion to electricity usually adopts two main methods: photovoltaic and solar-thermal power generation. Here, graphene-based thermionic-thermoradiative solar cells are expanded to include photovoltaics based on thermionic-thermoradiative converters, hybrid concept, efficiency limit, and optimum design. For realistic and practical design, a comprehensive and consistent model is formulated to include effects of thermal coupling between the absorbers, space-charge effect, non-radiative recombination, and various irreversible energy losses. By combining thermionic emission and thermoradiative mechanisms, thermionic-thermoradiative solar cells make use of electron and photon fluxes simultaneously to efficiently convert solar radiation to electricity, and thus enable a significant improvement in terms of heat utilization and conversion efficiency. Based on the calculated results, optimum choices of materials and the parametric design strategies of the system are determined. The findings predict a high solar-to-electricity efficiency of 0.225 in using a graphene-caesiated tungsten graphene-based thermionic energy converter and an Aluminium-32 gallium-48 arsenide-based thermoradiative cell under 800 sun irradiance. This work also demonstrates the importance of recycling waste heat for performance optimization and opens up new avenues to boost the overall conversion efficiency of such systems.

1. Introduction

Developing renewable energy is vital for a sustainable future (Sequeira et al., 2018). Serving as an abundant and clean energy source, solar energy shall play a significant role in powering economic growth and reducing global climate change (Crabtree et al., 2007; Mauleón, 2017). At present, photovoltaics (PV) (Chen et al., 2018) and solar thermal systems (Baljit et al., 2016) are the main technologies to convert sunlight into electricity. Solar energy conversion is performed mainly by distributed single-junction photovoltaic (PV) cells with conversion efficiencies constrained by the Shockley-Queisser limit to values below 40% that practically reduce to about 15% for modular systems (Shockley et al., 1961). The transition to higher-efficiency multijunction PV cells is currently hampered by the high cost per unit surface and by lack of homogeneity in material properties on large areas. Within a PV energy conversion process, photons with energies above the semiconductor bandgap can excite electrons into conduction band, subsequently, diffuse to charge-selective electrodes and contribute to electric current (Zhang et al., 2019a,b). In 2018, the worldwide cumulative photovoltaic installed capacity has exceeded 515 GW. The cell efficiency can be as high as 0.267 for mono-crystalline, meanwhile multi-crystalline silicon wafer-based solar cells yield a record of 0.223 (Green et al., 2018). Concentrating solar technologies represent economically viable alternatives to distributed PV since the optics production cost per unit surface is far lower than that of PV cells. The reduction of the active conversion area allows for expensive multijunction cells with efficiency as high as 45% to be used in concentrating PV. However, concentrating PV is struggling commercially because high-density arrangements are prevented by issues in excess heat removal (Dimroth et al., 2014). On the other hand, concentrating solar power technologies based on

* Corresponding author.
** Corresponding author.
E-mail addresses: jcchen@xmu.edu.cn (J. Chen), ricky_ang@sutd.edu.sg (L.K. Ang).

https://doi.org/10.1016/j.jclepro.2019.118444
0959-6526/

Nomenclature

A	Richardson constant in the metal
c	speed of light(cms^{-1})
C	solar concentration
e	Elementary charge(C)
E	Energy level (eV)
G	free carrier generation rate
I	solar irradiance (Wm^{-2}nm^{-1})
J	current density (Acm^{-2})
k	Boltzmann constant(eVK^{-1})
K	heat transfer coefficient(WK^{-1}cm^{-2})
P	power output density(Wcm^{-2})
q	heat flow density(Wcm^{-2})
r	reflection coefficient
R	free carrier recombination rate
T	temperature(K)
V	voltage output (V)

Greek symbols

$\hbar$	reduced Planck constant (eVs^{-1})
μ	sensitivity for the non-radiative process
η	efficiency
Φ	barrier height (eV)
ε	emissivity
ω	angular frequency
λ	wave length (cm)

Subscript

1	TIEC
2	TRC
A	anode of the TIEC
C	cathode of the TIEC
E	effective value
fe	electrons quasi-Fermi level
fh	holes quasi-Fermi level
FC	Fermi level of the cathode
FA	Fermi level of the anode
g	TRC bandgap
H	heat flow absorbed by the TIEC
L	radiation flow into environment
m	metal
M	maximum value
S	radiative energy flow from sun
SE(SA)	space-charge-induced barrier

Abbreviations

PV	photovoltaics
TIEC	thermionic emission converter
TRC	thermoradiative cell
TIRSC	thermionic-thermoradiative solar cell
SCE	space charge effect
NRR	Non-radiative recombination

transfer of high-temperature thermal energy through a fluid toward thermomechanical engines, are promising for large plants characterized by thermal-to-electric efficiency around 35%, with the important capabilities of energy cogeneration and storage (Pitz-Paal et al., 2013; Romero et al., 2012).

On the other hand, solar thermal system is applied to two practical ways, which includes practical light-to-electric power generation using mechanical heat engines in large-scale power plants and household heat supply through solar hot-water facilities. In such process, solar spectrum is first converted to high-temperature thermal energy and subsequently converted to electricity, and consequently, the entire solar spectrum can be utilized (Weinstein et al., 2015). This intermediate thermal procedure also provides a cheap alternative to store thermal energy (Weinstein et al., 2018).

Graphene-based thermionic emission converters (TIECs) (Liang et al., 2015; Zhang et al., 2017a,b) can convert part of supplied heat into electrical energy operating at relatively high temperatures (roughly 1200–2000 K), diffusing the electrons escape from the cathode fabricated with graphene and are subsequently absorbed by the metallic anode (Ang et al., 2018). Serving as emitter material for harvesting thermal energy, graphene can improve the capacity of electron emission attributing to its unique features such as excellent mobility (Sun et al., 2011), linear band structure (Novoselov et al., 2005), and superior thermal conductivity (Balandin et al., 2008). Despite several efforts regarding the TIEC have been reported (Xiao et al., 2017; Liao et al., 2019; Zhang et al., 2018a,b; Datas, 2016), to the best of the authors' knowledge, two major aspects missing from previous treatment of conversion efficiency include, the space charge effect (SCE) existing in such the two-electrode system and the determination of the electrode temperature from energy balances. Moreover, the TIEC anode usually operates at higher temperatures than ambient and the waste heat released from the TIEC is not generally utilized. These excess heat losses could be reclaimed by coupling with a secondary thermal engine, thus further improving the solar-energy conversion efficiency.

Nowadays, the potential of thermoradiative cell (TRC) (Lin et al., 2017; Liao et al., 2017) based on a p-n junction has been explored for moderate-grade waste-heat recovery, as experimentally demonstrated by Santhanam and Fan (Santhanam et al., 2016). Opposite to the PV cell, TRC, maintained at above ambient temperature, which operates as a microscale heat engine, and converts part of the supplied heat into electricity. Compared with conventional thermoelectric or thermophotovoltaics device, the TRC possesses the advantageous characteristics of high conversion efficiency and power generation (Strandberg et al., 2015). For example, a non-ideal TRC operated at temperature 800 K yields a maximum efficiency and power density up to 0.282 and 0.15 Wcm^{-2} (Zhang et al., 2017a,b). Matching well with the operating temperatures of TIEC, TRC could be a promising candidate for constituting a hybrid system together with a TIEC. Recent experimental progresses in the development of solar thermionic-thermoelectric generator has demonstrated graphene-based energy converter. For example, Trucchi et al. designed and fabricated a solar thermionic-thermoelectric generator, and demonstrated its concept, materials engineering, and prototype in details (Trucchi et al., 2018; Naito et al., 1996). Yuan et al. proposed the prototype TIEC with a backgated graphene anode, in which the maximum efficiency is 6.7 times higher than that of a TEC with a tungsten anode (Yuan et al., 2017). Santhanam and Fan demonstrated that the TRC under negative illumination can generate electric current, and then the theoretical limits of TRCs are analyzed (Santhanam et al., 2016). Ono et al. demonstrated the electric power generation from the coldness of the outer space through the negative illumination effect when an infrared semiconductor diode is oriented facing the sky (Ono et al., 2019). These pioneering experimental works offers a strong assurance to the feasibility of

graphene-based energy conversion proposed in this work, and further provides the critical first steps towards the industrial implementation of graphene-based TIRSC system for cleaner and more sustainable energy production in the near future.

Here, a stacked hybrid design of the graphene-based thermionic-thermoradiative solar cells (TIRSCs) is introduced, enabled by a spectrally selective absorber, a TIEC, operating at high but practical temperatures (<1500 K) that can be achieved with point-focus solar concentrators and the development of graphene, and with a TRC thermally connected in series. The TIRSC explored here takes the advantages of concentrating solar power and concentrating PV to provide an effective alternative concept for future solar technologies by combining the high-temperature operations, typical of concentrating solar power, to the compactness, scalability, reliability, and long operating lifetime of the solid-state converters, typically used in concentrating PV systems. Combining the key advantages of TIECs and TRCs, the TIRSC enables an obvious enhancement on the heat utilization and conversion efficiency at an extended range of solar concentration. Different from the thermionic energy converter for high-grade waste-heat recovery (Zhang et al., 2018a,b), this paper is focused on using concentrated solar cells to convert sunlight into electricity. Two physical effects that impact on the conversion efficiency of TIEC devices were not addressed in previous analyses (Xiao et al., 2017; Liao et al., 2019; Zhang et al., 2018a,b; Datas, 2016). These effects are explicitly considered in the improved computational modeling developed in this work. The first is the effect of space charge on the performance characteristics of a TIEC and the maximum power point. The second effect considered here is the thermal balance of the two electrodes. Using a generalized model, the optimal material to be used, and working parameters of the TIRSC are determined. These calculated results will be helpful for the optimum design and technological implementation of practical solar energy harvesting devices, thus providing more opportunities for the efficient utilization of solar energy. The solar cell explored here would operate at the temperature region exceeding 500 K, enabling its waste heat to be recycled to drive a secondary subcomponent TRC, and consequently, boosting theoretical combined conversion efficiencies above 0.20.

2. Materials and methods

Fig. 1 depicts the schematic diagram of the TIRSC containing a selective absorber, a TIEC, and a TRC. The TIEC includes a graphene-based cathode, a metallic anode, and a micron-scale vacuum gap between the two electrodes. Here monolayer graphene is used as the emitter of the TIEC mainly due to the fact that Graphene-based TIECs possess better performance than those using refractory metal as the emitter in the high temperature range (1200–1800 K) (Zhang et al., 2017a,b). Graphene can improve the capacity of electron emission attributing to its unique advantages, such as excellent mobility, high thermal stability (up till 4000 K), and superior thermal conductivity. The TRC, based on a p-n junction, is made of semiconductor materials. Facing the incoming sunlight, the wavelength-selective absorber harnesses the concentrated solar spectrum through the photonic crystal and transforms them into thermal energy (Nam et al., 2014). The absorbed heat is laterally conducted to the TIEC cathode to raise the cathode temperature, thus achieving heat-to-electricity conversion via thermionic emission. The TIEC anode would operate at temperatures exceeding 500 K as well as matching well with the temperature range of the TRC, so to allow the waste heat released from the anode to drive a secondary TRC to generate electricity. Finally, the low-grade heat produced in the TRC is released to the environment via thermal radiation and conduction. Thus, the TIRSC offers an alternative approach to heat recycling and performance enhancement for future concentrating solar thermal system.

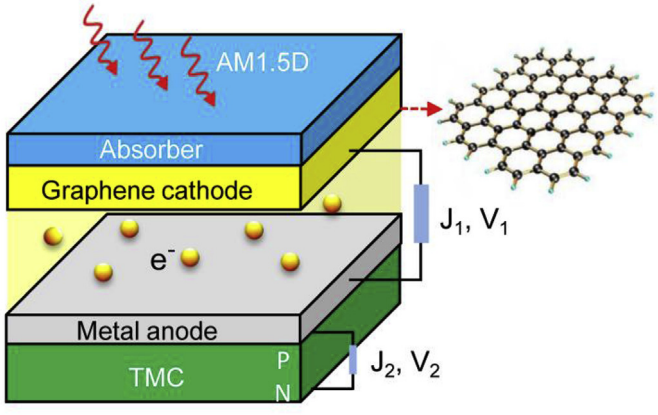

Fig. 1. The thermionic-thermoradiative solar cell with a stacked structure.

2.1. The absorber

In order to realize the cut-off absorber applicable for high operating temperatures, the radiative solar spectrum can be engineered using 2D tantalum photonic crystal (Nam et al., 2014). Tantalum is used as a promising candidate contributing to its high melting point (3290 K), low thermal emissivity and excellent solar absorptance (Shelton, 1957). At short wavelength regions (1–1.6 μm), it possesses lower emissivity than other low-emissivity materials (tungsten), which minimize radiative energy losses into environment (Nam et al., 2014). As the intermediate element between the solar concentrator and graphene cathode, the radiation absorber utilizes the concentrated broad solar spectrum and simultaneously converts them into heat. Here the absorber is assumed to have a uniform temperature T_C, and the thermal contact resistance between the absorber and the cathode are negligible. As indicated in Fig. 2, the energy balance equation for the absorber yields

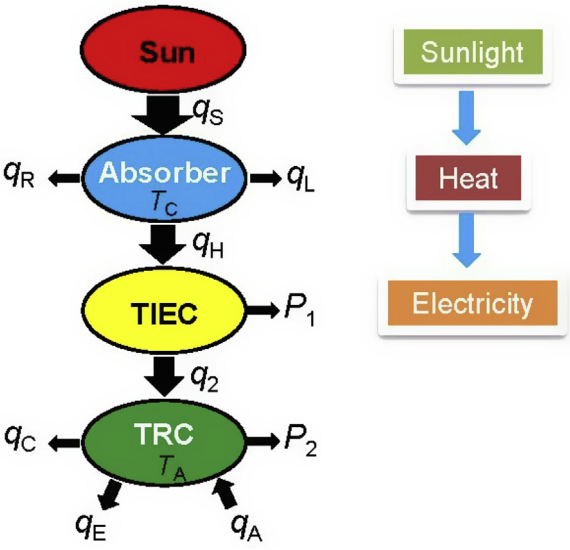

Fig. 2. The energy flow diagram for the TIRSC system.

$$q_S = q_H + q_L + q_R \tag{1}$$

where q_S represents the concentrated solar radiation flow density, q_H denotes the heat flows transferred to the TIEC cathode, q_R denotes the reflected radiation flow in the absorber, and q_L stands for the spectral blackbody emissive power density into the environment. Here, q_S, q_R, and q_L are, respectively, given by (Elzouka et al., 2017)

$$q_S = \eta_C C \int_0^\infty I_{AM1.5D}(\lambda) d\lambda \tag{2}$$

$$q_R = \eta_C C \int_0^\infty r(\lambda) I_{AM1.5D}(\lambda) d\lambda \tag{3}$$

and

$$q_L = \frac{2\pi hc^2}{\lambda^5} \int_0^\infty \varepsilon(\lambda)[\Theta(T_C) - \Theta(T_E)] d\lambda \tag{4}$$

where $I_{AM1.5D}(\lambda)$ represents the solar irradiance varying with the wavelength, whose corresponding radiation wavelength λ of AM1.5D solar spectrum is 0.28–4 μm (Emery, 2000), as shown in Fig. 3. The $\varepsilon(\lambda)$ denotes the spectral emissivity of the absorber surface, according to Kirchhoff law, which equals the spectral absorptance, and $r(\lambda) = 1 - \varepsilon(\lambda)$ stands for the reflection coefficient. Additionally, C is the concentration factor, η_C is the optical efficiency of the concentrator, and $\Theta(T) = (e^{hc/\lambda kT} - 1)^{-1}$ is the Bose-Einstein distributions of photons at the equilibrium temperature T.

2.2. Graphene-based TIECs

Graphene-based TIECs have the similar parallel-plate architecture as the traditional TIECs, except for monolayer graphene as the cathode. Different from the previous literature (Liang et al., 2015; Zhang et al., 2017a,b), the effect of space charge between two electrodes on the performance of a micron-scale-gap TIEC should be considered. In this case, with the increasing of the vacuum-gap width, the space charge effect occurring in the vacuum gap distinctly reduces the performance of the TIEC (Lee et al., 2012; Su et al., 2014; Zhang et al., 2018a,b). Fig. 4(A) depicts the energy level diagram of a TIEC, where Φ_C and Φ_A are the work functions of the graphene and metal, respectively. Φ_{SC} and Φ_{SA} are the additional barriers due to space charge effects between the electrodes and can be calculated by using the space charge limited current model (Lee et al., 2012). The voltage output is given by $eV_1 = (\Phi_C + \Phi_{SC}) - (\Phi_A + \Phi_{SA}) = E_{FA} - E_{FC}$, where E_{FC} and E_{FA} are the Fermi level of the cathode and anode. The position-dependent potential distribution $\Phi(x)$ along with the x direction yields the maximum value Φ_M. The vacuum gap is set to be micrometer regime, i.e., $D = 2$ μm, in order to weaken the space charge effect and realize a high energy conversion efficiency (Hishinuma et al., 2001; Su et al., 2014).

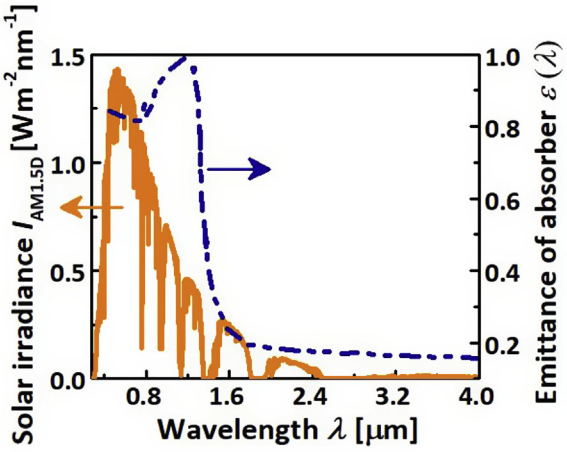

Fig. 3. The direct solar irradiance and emittance of an absorber varying with wavelength.

Thermionic emission in the TIEC is a three-step process. Firstly, the cathode absorbs the heat flow q_H and electrons existing in the graphene rapidly thermalize to an equilibrium heat distribution. Secondly, the electrons with energy larger than Φ_M can overcome surface barrier of the graphene to be emitted into the vacuum gap by thermionic emission. Finally, these electrons condense at the anode across the vacuum gap. For 2D materials such as graphene, electrons behave like the massless Dirac fermion and have a linear energy momentum dispersion relation. Moreover, the out-of-plane electron transport due to electron-electrons interaction, interface inhomogeneities, and substrate effect between graphene and Tantalum are excluded. Consequently, the current density emitted from the cathode due to the revised thermionic emission law is given as follows (Liang et al., 2015; Zhang et al., 2017a,b; Ang et al., 2018):

$$J_C = \frac{ek^3 T_C^3}{\pi^2 \hbar^3 v_F^2} \exp\left(-\frac{\Phi_C + \Phi_{SC}}{kT_C}\right) = \frac{ek^3 T_C^3}{\pi^2 \hbar^3 v_F^2} \exp\left(-\frac{\Phi_M - E_{FC}}{kT_C}\right) \tag{5}$$

where e is the elementary charge, $\hbar$ is the reduced Planck constant, k is the Boltzmann constant, and v_F represents the velocity of massless Dirac fermions in the graphene. The current density emitted by the metals at the anode obeys the traditional Richadson-Dushman law as

$$J_A = AT_A^2 \exp\left(-\frac{\Phi_A + \Phi_{SA}}{kT_A}\right) = AT_A^2 \exp\left(-\frac{\Phi_M - E_{FA}}{kT_A}\right) \tag{6}$$

where A is the Richardson constant depending on electron mass, T_A is the anode temperature. The net current density J_1 generated by TIEC is the difference between the thermionic current densities from the cathode and anode $J_1 = J_C - J_A$. Thus, the power density of the TIEC can be given by

$$P_1 = J_1 V_1 = (J_C - J_A)(E_{FA} - E_{FC})/e \tag{7}$$

To find the optimum values for three independent parameters, namely Φ_M, E_{FC}, and $E_{FA}$for maximum power generation, it is possible to reduce the problem to two parameters without the loss of generality, by the following observation. To quantitatively describe the system performance, a generalized parameter Φ_E is introduced, where Φ_E denotes the effective barrier in the graphene-based cathode and is determined by the graphene work function Φ_C, Fermi level E_{FC}, space-charge-induced barrier Φ_{SC}, and some other effects in the gap. Setting $\Phi_M - E_{FC} = \Phi_E$ and $\Phi_M - E_{FA} = \Phi_E - V_1$, as shown in (5–7), only Φ_E and V_1 have to be varied in order to maximize the power output density.

2.3. Negative illumination thermoradiative cells

The p-n-junction-based TRC can convert the thermal energy into the electricity via photon exchange with surroundings under

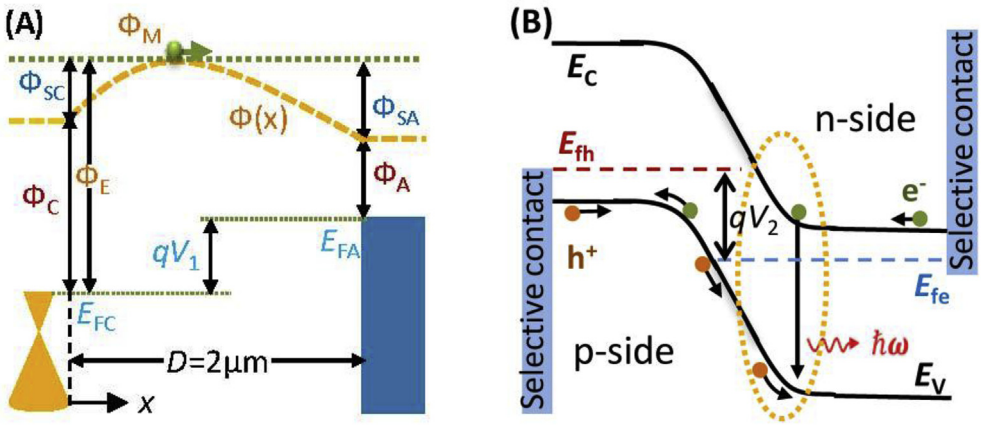

Fig. 4. Band diagram of (A) a graphene-based TIEC with the SCE and (B) a TRC showing a transfer route for electrons and holes.

negative illumination. Fig. 4(B) describes the transferring process of the electrons and holes within the TRC. By elevating the operating temperatures, the p-n junction shall radiate more photons than it absorbs. Consequently, it will produce an opposite electric current, which is contrasted with the current direction of the PV cell. In a realistic TRC, the sub-bandgap radiation and non-radiative process (Pidgeon et al., 1997; Virgilio et al., 2015) should be considered as an additional loss mechanism. The net radiative heat flow carried by the sub-bandgap photons makes no contribution to the power output and decreases the efficiency. This issue can be remedied by placing an optical filter at the backsides of the cell for sub-bandgap photon-recycling. Non-radiative loss contributes to the net carrier generation via Auger, surface defect, and Shockley-Read-Hall processes (Ley et al., 2005; Zhang et al., 2019a,b). Moreover, compared with the Auger process, the effect of Shockley-Read-Hall and surface defect processes on the electric current can be neglected (Hsu et al., 2016). Following the detailed balance formalism and considering the non-radiative loss, the total current density generated in the TRC can be calculated as follows:

$$J_2 = e(\mu G_{\mathrm{rad}} - R_{\mathrm{rad}}) \tag{8}$$

where μ represents a dimensionless parameter that characterizes the relative strength between the radiative and non-radiative processes (Lin et al., 2017; Strandberg et al., 2015; Zhang et al., 2017a,b). This parameter has included all effects, such as cell temperature dependence, thickness dependence, carrier concentration, etc. Generally, the smaller the parameter μ, the better the performance of the TRC achieves (Zhang et al., 2017a,b). As a special example, here $\mu = 20$ is used in the calculations, which means radiative excitation contributing to 20% of the total excitation rate. $G_{\mathrm{rad}}$and R_{rad} correspond to the free carrier generation and recombination rates due to the radiative process, which are expressed as

$$G_{\mathrm{rad}} = \int_{\omega_g}^{\infty} \frac{\omega^2}{4\pi^2 c^2} \Theta(T_{\mathrm{E}}, 0) d\omega \tag{9}$$

and

$$R_{\mathrm{rad}} = \int_{\omega_g}^{\infty} \frac{\omega^2}{4\pi^2 c^2} \Theta(T_{\mathrm{A}}, qV_2) d\omega \tag{10}$$

where ω represents the angular frequency of photons. Hence, the power output density produced in the TRC can be written as $P_2 = J_2V_2$. Here E_g and V_2 are varied to obtain the maximized power output density for a given temperature.

3. Temperature determination and conversion efficiency

As shown in Fig. 2, the TRC emits the radiative energy flow density q_{E} into the surrounding and simultaneously absorbs the radiative energy flow density q_{A} from the ambient environment, while produces the power output densityP_2 and heat flows q_{C} into the environment through heat conduction. Based on the first law of thermodynamics, the energy balance equations for the cathode, anode, and TRC are given by

$$q_{\mathrm{H}} - \frac{J_{\mathrm{C}}(\Phi_{\mathrm{M}} - E_{\mathrm{FC}} + 2kT_{\mathrm{C}})}{e} + \frac{J_{\mathrm{A}}(\Phi_{\mathrm{M}} - E_{\mathrm{FC}} + 2kT_{\mathrm{A}})}{e} - \varepsilon_{\mathrm{e}}\sigma\left(T_{\mathrm{C}}^4 - T_{\mathrm{A}}^4\right) = 0 \tag{11}$$

$$\frac{J_{\mathrm{C}}(\Phi_{\mathrm{M}} - E_{\mathrm{FA}} + 2kT_{\mathrm{C}})}{e} - \frac{J_{\mathrm{A}}(\Phi_{\mathrm{M}} - E_{\mathrm{FA}} + 2kT_{\mathrm{A}})}{e} + \varepsilon_{\mathrm{e}}\sigma\left(T_{\mathrm{C}}^4 - T_{\mathrm{A}}^4\right) - q_2 = 0 \tag{12}$$

and

$$q_2 = q_{\mathrm{E}} + q_{\mathrm{C}} + P_2 - q_{\mathrm{A}} \tag{13}$$

The second term within Eq. (11) denotes the energy flux density carried by electrons leaving the cathode, while the third term represents the energy flux from the anode to the cathode. Similarly, in Eq. (12), the first and second terms corresponds the electron flux flowing into and leaving the anode, respectively. $q_{\mathrm{C}} = K(T_{\mathrm{C}} - T_{\mathrm{E}})$ and K is the heat transfer coefficient. $q_{\mathrm{A}} - q_{\mathrm{E}} = \hbar\omega \cdot e(G_{\mathrm{rad}} - R_{\mathrm{rad}})$ is the net radiative energy flux flowing into environment. Here, ε_{e} is the effective emissivity between the graphene cathode with an emittance of ε_{R} (Mak et al., 2008; Muley et al., 2014; Berciaud et al., 2010) and the metallic anode with an emittance of ε_{m}, which can be calculated from (Kraemer et al., 2011)

$$\varepsilon_{\mathrm{e}} = \left(1/\varepsilon_{\mathrm{g}} + 1/\varepsilon_{\mathrm{m}} - 1\right)^{-1} \tag{14}$$

Following recent absorption measurements, the emissivity of a graphene monolayer is assumed as a constant (2.3%) (Mak et al., 2008; Muley et al., 2014; Berciaud et al., 2010). For simplicity, the

effects of substrate and temperature on the material emissivity are ignored. It should be noted that, in general, the emissivity of graphene can behave differently for different substrates, such as silicon, hBN, tungsten, and tantalum, and is also dependent on wavelength, layers of graphene, and temperature (Mak et al., 2008; Muley et al., 2014). For simplicity, such effects are neglected in the modeling of graphene emissivity.

Solving (1–4) and (11–14), the temperatures of the absorber-cathode and the anode-TRC interfaces, i.e. T_C and T_A can be determined. The total electric power density is the sum of the power densities generated by the TIEC and TRC, i.e. $P_1 + P_2$. Thus, the overall efficiency of the TIRSC is calculated by

$$\eta = \frac{P_1 + P_2}{q_S} = \frac{J_1 V_1 + J_2 V_2}{C \int_0^\infty I_{AM1.5D}(\lambda) d\lambda} \tag{15}$$

The maximum power density is calculated by maximizing $J_1 V_1$ and $J_2 V_2$, with the respective optimal values of Φ_E, V_1 , E_g and V_2. For optimal performance to be achieved in the TIRSC, it is useful to consult a simply generalized model including these four parameters. The fixed parameters used for the generalized model are summarized in Table I.

4. Results and discussion

The performance of a TIRSC is a strong function of the TIEC effective barrier Φ_E and TRC bandgap E_g. With this generalized model, material configurations in co-generation system can be explored. Fig. 5(A) shows the overall conversion efficiency η of the TIRSC by varying effective barriers and bandgaps. The maximal efficiency of 0.225 occurs for an effective barrier of 3.83 eV and a TRC bandgap of 0.0901 eV, which corresponds to the operating temperature for the cathode of 2687 K and the anode of 803 K, and the voltage output of 1.88 V for the TIEC and −0.042 V for the TRC, respectively. Under the 800 solar concentration, the efficiency of this new concept concentrating solar cell can reach 0.225. Although the efficiency is far below the Carnot efficiency limit of 0.701, the TIRSC still has the better performance than high-performance solar thermionic-thermoelectric generator with a peak efficiency of 0.046 (Kraemer et al., 2011) and 0.06 (Trucchi et al., 2018). For a full solar thermophotovoltaic device, which, thanks to the nano-photonic properties of the absorber–emitter surface, reaches experimental efficiencies of 0.032. Moreover, the cell efficiency can be as high as 0.267 for mono-crystalline, meanwhile multi-crystalline silicon wafer-based solar cells yield a record of 0.223 (Green et al., 2018). However, there is no need to shed negative light on the TIRSC system because this new technology still provides a viable alternative to solar harvesting technology. Furthermore, this 2D material approach opens up a new route, potentially can be further improved using properly designed van der Waals heterostructure.

According to the optimal values of the effective barrier, voltage output, and operating temperature, appropriate materials as electrodes in the TIEC can be chosen. For example, one can select the graphene with the effective barrier 3.83 eV as the cathode and caesiated tungsten with the work function of 1.95 eV as the anode. The graphene with effective barrier of 3.83 eV can be achieved by engineering the work function and Fermi level. Experimentally, the Fermi level can be tuned over a broad range around 0.5–0.85 eV via chemical doping (Giovannetti et al., 2008) and electrostatic gate voltage (Lee et al., 2015). Moreover, experimentally, coating materials with alkali or alkali-earth metals can engineer to lower the work function, most notably cesium. Considering the alignment of the bandgap induced by the temperature dependence, Aluminium gallium arsenide ($Al_{32}Ga_{48}As$ compounds) (Steranka, 1997) with an energy band gap of 1.519 eV at 0 K and a melting point of above 1200 K is selected as the promising material for the TRC.

The general approach employed to obtain the optimal effective barrier in graphene and the semiconductor bandgap in the TRC for achieving maximum system efficiency is now discussed. In general, the effective barriers in graphene should be as small as possible to maximize electron emission. However, due to the presence of the heat exchange with the ambient environment, the optimal value of the effective barrier exhibits a complex interplay between the maximum current density J_1 and the voltage output V_1, as shown in Fig. (7) below. The TIRSC conversion efficiency depends on the output power produced by the TRC, which is a product of the output current J_2 and the output voltage V_2. For large-bandgap materials, although the output voltage is strongly improved due to the large quasi-Fermi level mismatch, the photon absorption and emission are significantly impeded by large bandgap leading to a small electrical current. For small-bandgap materials, although a larger electrical current is warranted, the output voltage remains low. Thus, the interplays between these two aspects will lead to an optimal bandgap for achieving maximum conversion efficiency (Zhang et al., 2019a,b).

As shown in Fig. 5(B), the cathode temperature first decreases and then increases with the increment of the effective barrier. It is however rarely affected by the TRC bandgap, which can be simply explained by (11). For high (low) effective barrier, less (more) electrons are emitted by the cathode, allowing high temperatures to satisfy the energy balance in the cathode. Additionally, Fig. 5(C) shows that the anode-TRC temperature decreases with the effective barrier, while increases with the bandgap. Since the anode temperature is closely dependent on the emitted energy fluxes from the cathode and into the environment, these energy fluxes will decrease at higher effective barriers and lower bandgaps, which leads to the smaller amount of heat to the anode and lower anode temperature.

As expected in most solar thermal systems, Fig. 6(A) shows that higher concentration will lead to higher efficiency (Kylili et al., 2018). The efficiency predicted in the generalized model illustrates that the TIRSC can serve as a capable candidate for harvesting solar energy, since it achieves higher efficiency than a TIEC-only

Table 1
Parameters used in the generalized model.

Symbol	Property	Value
η_C	Optical efficiency for the solar concentrator [21]	0.95
v_F	Velocity of massless Dirac fermions in the graphene [10]	$10^8 cms^{-1}$
A	Richardson constant in the metal	$120 Acm^{-2}K^{-2}$
K	Heat transfer coefficient [11]	$0.2 \times 10^{-2} Wcm^{-2}K^{-1}$
ε_g	Emittance for graphene [35–37]	2.3%
ε_m	Emittance for metal [11]	0.05
T_E	Ambient temperature	300K
μ	Sensitivity of TRCs for non-radiative process [23, 24]	20

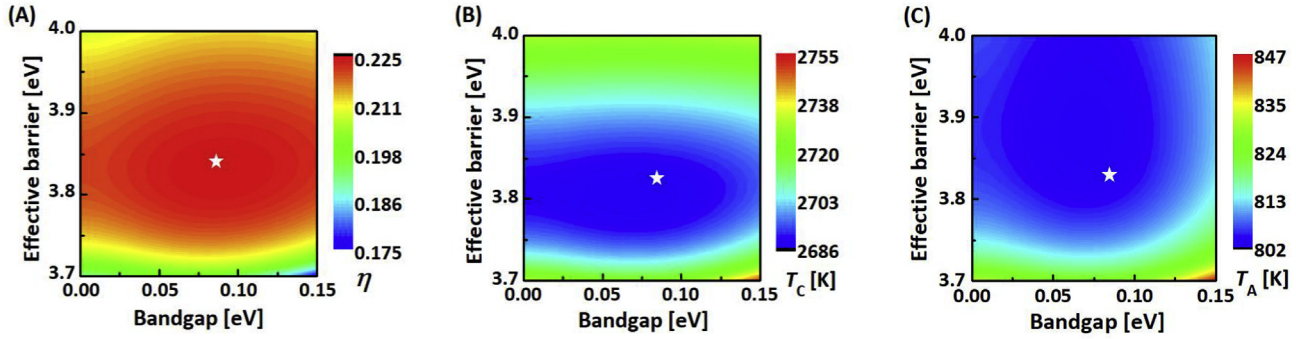

Fig. 5. The performance of a TIRSC as predicted by the normalized model. (A) The overall efficiency, (B) the cathode temperature, and (C) the anode temperature as a function of the TIEC effective barrier and TRC band gap under 800 solar concentration, where the voltage outputs of the TIEC and TRC have been optimized for maximum efficiency. Star denotes the maximum efficiency of 22.5%.

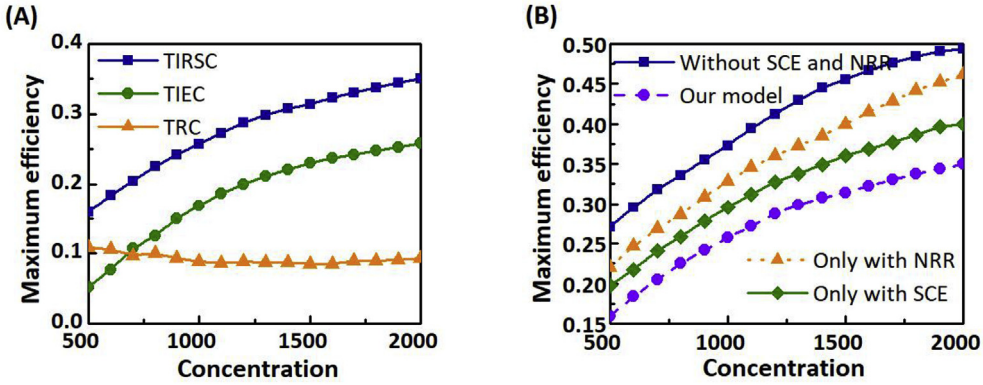

Fig. 6. The optimal performance of the system varies with the solar concentration factor. (A) The comparisons of maximum efficiencies among the TIRSC, TIEC, and TRC. (B) The maximum efficiencies in four cases, i.e., without the SCE and NRR; The proposed model; Only with the NRR; Only with the SCE.

system. Particularly, under the 500 solar irradiance, a TIRSC yields a 16% solar-to-electricity conversion efficiency, which is a 2.2X performance improvement as compared with TIEC. This implies that the TIRSC possesses a better performance in an extended concentration range. For low concentration, the TIRSC performs like the TRC due to the negligible electron flux in the TIEC. On the contrary, for high concentration, the TIRSC behaves like the TIEC, originating from great enhancement of the electron flux overshadows the photon flux contribution in the TRC. Moreover, the energy loss mechanisms in the TIRSC are further explored, as shown in Fig. 6(B), where the system only with the NRR corresponds to the case of the linear potential distribution in the vacuum gap of the TIEC and the system only with the SCE means that the TRC is made of ideal semiconductor materials. The effects of the NRR and SCE on the performance of the solar cells are analyzed to identify the dominant loss contributors that restricts the overall efficiency of the TIRSC. For example, under 500 concentration, the SCE and NRR could lead to 7.6% and 6.3% performance degradations in contrast to the ideal case without these effects. It indicates that the SCE plays the most critical role in degrading the system performance, and more efforts should be paid to reduce its effects (Su et al., 2014). As a result, early TIECs used ignited cesium plasma to neutralize space charge between the electrodes in the 1950s–1980s. Such plasma TIECs achieved high power output, but only at the cost of greatly increased complexity and decreased maximum efficiency (Shefsiek, 2010). As an alternative to using plasma, the deleterious effects of space charge can also be mitigated by making the interelectrode gap small enough so that there is not enough space to develop a significant additional energy barrier. It has long been known that such vacuum TIECs can be more efficient than plasma TIECs if micron-scale gaps are used (<10 μm). This fact has been a motivation for recent efforts to develop microfabricated thermionic energy converters (Khalid et al., 2016).

In general, a larger concentration factor corresponds to a larger input energy flux, and a higher electrode temperature corresponds to a larger current density (Kylili et al., 2018). Thus, the optimum values of T_C, T_A, J_1, and $|J_2|$under the maximum efficiency, monotonically increase with the concentration, as shown in Fig. 7(A) and (B). However, in Fig. 7(C) the optimum cathode barrier and TRC bandgap are not a monotonic function of concentration and have the maximum value 3.85 eV and 0.165 eV under the condition of 900 and 1000 solar irradiance, respectively. The TIRSC performance data obtained from Figs. 5–7 shall offer a practical design of high-performance TIRSCs, thus paving the way towards the development of future concentrating solar plants (Sadi et al., 2019).

5. Conclusions and future work

Based on the thermionic-thermoradiative energy conversion mechanisms, a new-concept of solar thermal energy conversion system coupled to photovoltaics is proposed here, which can efficiently convert solar energy into electricity. As the TIRSC is a solid-state-based energy converter, the device exhibits long lifetimes, contains no moving parts, and can be scaled-up to larger system. Based on the calculation, such a TIRSC may yield a high solar-to-electric conversion efficiency of 0.225 under 800 sun irradiance, which is comparable to multi-crystalline silicon wafer-based solar cells with 0.223 efficiency. Note the self-consistent model of the

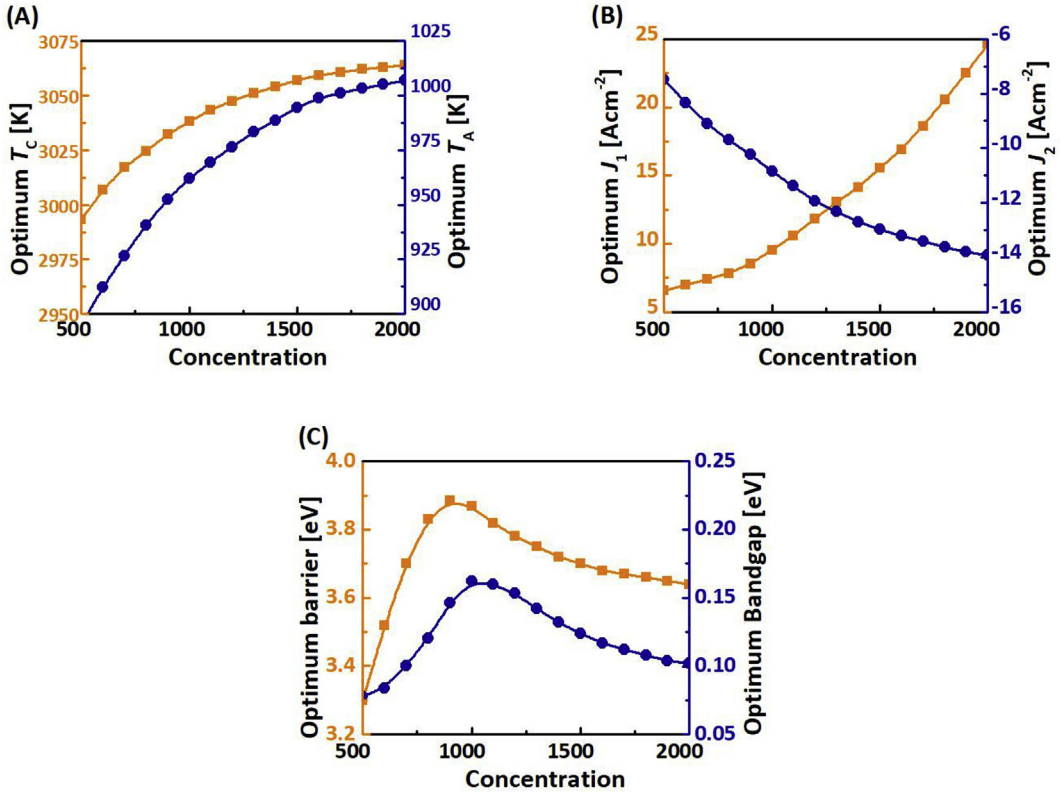

Fig. 7. The optimum (A) electrode temperature T_C and T_A, (B) current density J_1 and J_2, and (C) effective barrier in the TIEC and TRC bandgap under different concentrations.

TIRSC proposed here has included some important non-ideal factors missing from the previous treatment, such as the space charge effect, non-radiative recombination, and other irreversible losses. This model shall provide important guidelines for future experimental design of the TIRSC, which is beyond the scope of this work. Under this generalized framework, the upper bound of efficiency limit, the choice of electrode materials, and the optimally working conditions under different solar concentrations are estimated. Under the 500 solar irradiance, the proposed TIRSC will enable a 2.2 times performance improvement compared to the subcomponent TIEC. This highlights the advantageous of TIRSC system for high-efficiency heat utilization. Technically, it is found that NRR and SCE are the two dominant loss contributors that severely restricts the overall efficiency of the TIRSC. These results will provide important guideline for the experimental realization of TIRSCs and sheds new light on the implementation of 2D materials in cleaner production and sustainable development for energy harvesting.

Direct high-efficiency conversion from solar thermal energy to electricity represents one of the promising energy sources for both earth-based and space-based consumption in the future. One important advantage of the concentrating solar power systems is that they can be integrated straightforwardly with other existing fossil fuels, such as natural gas, so that additional investments in the power block and transmission lines can be reduced to obtain significant cost reduction while increasing the energy efficiency. The TIRSC explored here takes the advantages of TIEC and TRC to provide an effective alternative concept for future solar harvesting technologies, which combines the long operating lifetime, high power generation, and the energy conversion efficiency of solid-state energy converters. As an environmentally sustainable energy system, the proposed TIRSC can help to reduce the reliance on fossil fuel, to reduce the pollutants and carbon emissions, and to meet the requirements of economic cost-effectiveness, thus relieving the many operational stresses of the main power network system.

Acknowledgments

This work was supported by the National Natural Science Foundation of China under Grant 11675132 and Fundamental Research Fund for the Central Universities under Grant 20720180011, People's Republic of China, and Singapore A*STAR AME IRG under Grant A1783c0011.

Appendix A. Supplementary data

Supplementary data to this article can be found online at https://doi.org/10.1016/j.jclepro.2019.118444.

Conflicts of interest

There are no conflicts to declare.

References

Ang, Y.S., Yang, H.Y., Ang, L.K., 2018. Universal scaling laws in Schottky heterostructures based on two dimensional materials. Phys. Rev. Lett. 121, 056802.
Balandin, A.A., Ghosh, S., Bao, W., Calizo, I., Teweldebrhan, D., Miao, F., Lau, C.N., 2008. Superior thermal conductivity of single layer graphene. Nano Lett. 8, 902–907.
Baljit, S.S.S., Chan, H.Y., Sopian, K., 2016. Review of building integrated applications of photovoltaic and solar thermal systems. J. Clean. Prod. 137, 677–689.
Berciaud, S., Han, M.Y., Mak, K.F., Brus, L.E., Kim, P., Heinz, T.F., 2010. Electron and optical phonon temperatures in electrically biased graphene. Phys. Rev. Lett. 104, 227401.
Chen, H., Ji, J., Pei, G., Yang, J., Zhang, Y., 2018. Experimental and numerical comparative investigation on a concentrating photovoltaic system. J. Clean.

Prod. 174, 1288–1298.
Crabtree, G.W., Lewis, N.S., 2007. Solar energy conversion. Phys. Today 60, 37–42.
Datas, A., 2016. Hybrid thermionic-photovoltaic converter. Appl. Phys. Lett. 108, 143503.
Dimroth, F., Grave, M., Beutel, P., Fiedeler, U., Karcher, C., Tibbits, T.N.D., Oliva, E., Siefer, G., Schachtner, M., Wekkeli, A., Bett, A.W., Krause, R., Piccin, M., Blanc, N., Drazek, C., Guiot, E., Ghyselen, B., Salvetat, T., Tauzin, A., Signamarcheix, T., Dobrich, A., Hannappel, T., Schwarzburg, K., 2014. Wafer bonded four-junction GaInP/GaAs//GaInAsP/GaInAs concentrator solar cells with 44.7% efficiency. Prog. Photovolt. Res. Appl. 22, 277.
Elzouka, M., Ndao, S., 2017. Towards a near-field concentrated solar thermophotovoltaic microsystem: Part I—Modeling. Sol. Energy 141, 323–333.
Emery, K., 2000. Reference Solar Spectral Irradiance. *Amer. Soc. Test. Mater.* (ASTM), Conshohocken, PA, USA. NREL Rep. CP-520-28860. [Online]. Available. http://rredc.nrel.gov/solar/spectra/am1.5/.
Giovannetti, G., Khomyakov, P.A., Brocks, G., Karpan, V.M., van den Brink, J., Kelly, P.J., 2008. Doping graphene with metal contacts. Phys. Rev. Lett. 101, 026803.
Green, M.A., Hishikawa, Y., Dunlop, E.D., Levi, D.H., Hohl-Ebinger, J., Ho-Baillie, A.W.Y., 2018. Solar cell efficiency tables (version 52). Prog. Photovolt. Res. Appl. 26, 427–436.
Hishinuma, Y., Geballe, T.H., Moyzhes, B.Y., Kenny, T.W., 2001. Refrigeration by combined tunneling and thermionic emission in vacuum: use of nanometer scale design. Appl. Phys. Lett. 78, 2572–2574.
Hsu, W.-C., Tong, J.K., Liao, B., Huang, Y., Boriskina, S.V., Chen, G., 2016. Entropic and near-field improvements of thermoradiative cells. Sci. Rep. 6, 3483.
Khalid, K.A.A., Leong, T.J., Mohamed, K., 2016. Review on thermionic energy converters. IEEE Trans. Electron Devices 63, 2231–2241.
Kraemer, D., Kraemer, D., Poudel, B., Feng, H.P., Caylor, J.C., Yu, B., Yan, X., Ma, Y., Wang, X., Wang, D., Muto, A., McEnaney, K., Chiesa, M., Ren, Z., Chen, G., 2011. High-performance flat-panel solar thermoelectric generators with high thermal concentration. Nat. Mater. 10, 532–538.
Kylili, A., Fokaides, P.A., Ioannides, A., Kalogirou, S., 2018. Environmental assessment of solar thermal systems for the industrial sector. J. Clean. Prod. 176, 99–109.
Lee, E.J., Choi, S.Y., Jeong, H., Park, N.H., Yim, W., Kim, M.H., Park, J.-K., Son, S., Bae, S., Kim, S.J., Lee, K., Ahn, Y.H., Ahn, K.J., Hong, B.H., Park, J.-Y., Rotermund, F., Yeom, D., 2015. Active control of all-fiber graphene devices with electrical gating. Nat. Commun. 6, 6851.
Lee, J.H., Bargatin, I., Melosh, N.A., Howe, R.T., 2012. Optimal emitter-collector gap for thermionic energy converters. Appl. Phys. Lett. 100, 173904.
Ley, M., Boudaden, J., Kuznicki, Z.T., 2005. Thermodynamic efficiency of an intermediate band photovoltaic cell with low threshold Auger generation. J. Appl. Phys. 98, 044905.
Liang, S.J., Ang, L.K., 2015. Electron thermionic emission from graphene and a thermionic energy converter. Phys. Rev. Appl. 3, 014002.
Liao, T., 2019. Improved design of a photon enhanced thermionic energy converter. IEEE Electron. Device Lett. 40, 115–118.
Liao, T., Zhang, X., Chen, X., Lin, B., Chen, J., 2017. Negative illumination thermoradiative solar cell. Opt. Lett. 42, 3236–3238.
Lin, C., Wang, B., Teo, K.H., Zhang, Z., 2017. Performance comparison between photovoltaic and thermoradiative devices. J. Appl. Phys. 122, 243103.
Mak, K.F., Sfeir, M.Y., Wu, Y., Lui, C.H., Misewich, J.A., Heinz, T.F., 2008. Measurement of the optical conductivity of graphene. Phys. Rev. Lett. 101, 196405.
Mauleón, I., 2017. Photovoltaic investment roadmaps and sustainable development. J. Clean. Prod. 167, 1112–1121.
Muley, S.V., Ravindra, N.M., 2014. Emissivity of electronic materials, coatings, and structures. J. Occup. Med. 66, 616–636.
Naito, H., Kohsaka, Y., Cooke, D., Arashi, H., 1996. Development of a solar receiver for a high-efficiency thermionic/thermoelectric conversion system. Sol. Energy 58, 191–195.
Nam, Y., Yeng, Y.X., Lenert, A., Bermel, P., Celanovic, I., Soljačić, M., Wanga, E.N., 2014. Solar thermophotovoltaic energy conversion systems with two-dimensional tantalum photonic crystal absorbers and emitters. Sol. Energy Mater. Sol. Cells 122, 287–296.
Novoselov, K.S., Geim, A.K., Morozov, S.V., Jiang, D., Katsnelson, M.I., Grigorieva, I.V., Dubonos, S.V., Firsov, A.A., 2005. Two-dimensional gas of massless Dirac fermions in graphene. Nature 438, 197–200.
Ono, M., Santhanam, P., Li, W., Zhao, B., Fan, S., 2019. Experimental demonstration of energy harvesting from the sky using the negative illumination effect of a semiconductor photodiode. Appl. Phys. Lett. 114, 161102.
Pidgeon, C.R., Ciesla, C.M., Murdin, B.N., 1997. Suppression of non-radiative processes in semiconductor mid-infrared emitters and detectors. Prog. Quantum Electron. 21, 361–419.
Pitz-Paal, R., Amin, A., Bettzuge, M., Eames, P., Fabrizi, F., Flamant, G., Novo, F.G., Holmes, J., Kribus, A., Van der Laan, H., Lopez, C., Papagiannakopoulos, P., Pihl, E., Smith, P., Wagner, H.-J., 2013. Concentrating solar power in Europe, the Middle East and North Africa: achieving its potential. J. Energy Power Eng. 7, 219.
Romero, M., Steinfeld, A., 2012. Concentrating solar thermal power and thermochemical fuels. Energy Environ. Sci. 5, 9234.
Sadi, M., Arabkoohsar, A., 2019. Modelling and analysis of a hybrid solar concentrating-waste incineration power plant. J. Clean. Prod. 216, 570–584.
Santhanam, P., Fan, S., 2016. Thermal-to-electric energy conversion by diodes under negative illumination. Phys. Rev. B 93, 161410.
Sequeira, T.N., Santos, M.S., 2018. Renewable energy and politics: a systematic review and new evidence. J. Clean. Prod. 192, 553–568.
Shefsiek, P., 2010. Describing and correlating the performance of the thermionic converter: a historical perspective. IEEE Trans. Plasma Sci. 38, 2041–2047.
Shelton, H., 1957. Thermionic emission from a planar tantalum crystal. Phys. Rev. 107, 1553.
Shockley, W., Queisser, H.J., 1961. Detailed balance limit of efficiency of p-n junction solar cells. J. Appl. Phys. 32, 510–519.
Steranka, F.M., 1997. AlGaAs red light-emitting diodes. Semiconduct. Semimet. 48, 65–96.
Strandberg, R., 2015. Theoretical efficiency limits for thermoradiative energy conversion. J. Appl. Phys. 117, 055105.
Su, S., Wang, Y., Liu, T., Su, G., Chen, J., 2014. Space charge effects on the maximum efficiency and parametric design of a photon-enhanced thermionic solar cell. Sol. Energy Mater. Sol. Cells 121, 137–143.
Sun, S., Ang, L.K., Shiffler, D., Luginsland, J.W., 2011. Klein tunneling model of low energy electron field emission from single-layer graphene sheet. Appl. Phys. Lett. 99, 013112.
Trucchi, D.M., Bellucci, A., Girolami, M., Calvani, P., Cappelli, E., Orlando, S., Polini, R., Silvestroni, L., Sciti, D., Kribus, A., 2018. Solar thermionic-thermoelectric generator (ST^2G): concept, materials engineering, and prototype demonstration. Adv. Energy Mater. 8, 1802310.
Virgilio, M., Schroeder, T., Yamamoto, Y., Capellini, G., 2015. Radiative and non-radiative recombinations in tensile strained Ge microstrips: Photoluminescence experiments and modeling. J. Appl. Phys. 118, 233110.
Weinstein, L.A., Loomis, J., Bhatia, B., Bierman, D.M., Wang, E.N., Chen, G., 2015. Concentrating solar power. Chem. Rev. 115, 12797–12838.
Weinstein, L.A., McEnaney, K., Strobach, E., Yang, S., Bhatia, B., Zhao, L., Huang, Y., Loomis, H., Cao, F., Boriskina, S.V., Ren, Z., Wang, E.N., Chen, G., 2018. A hybrid electric and thermal solar receiver. Joule 2, 962–975.
Xiao, G., Zheng, G., Qiu, M., Li, Q., Li, D., Ni, M., 2017. Thermionic energy conversion for concentrating solar power. Appl. Energy 208, 1318–1342.
Yuan, H., Riley, D.C., Shen, Z.X., Pianetta, P.A., Melosh, N.A., Howe, R.T., 2017. Back-gated graphene anode for more efficient thermionic energy converters. Nano Energy 32, 67–72.
Zhang, X., Ang, Y.S., Chen, J., Ang, L.K., 2019a. Design of an InSb thermoradiative system for harvesting low-grade waste heat. Opt. Lett. 44, 3354–3357.
Zhang, X., Ang, Y.S., Ye, Z., Su, S., Chen, J., Ang, L.K., 2019b. Three-terminal heterojunction bipolar transistor solar cells with non-ideal effects: efficiency limit and parametric optimum selection. Energy Convers. Manag. 188, 112–119.
Zhang, X., Pan, Y., Chen, J., 2017a. Parametric optimum design of a graphene-based thermionic energy converter. IEEE Trans. Electron Devices 64, 4594–4598.
Zhang, X., Peng, W., Lin, J., Chen, X., Chen, J., 2017b. Parametric design criteria of an updated thermoradiative cell operating at optimal states. J. Appl. Phys. 122, 174505.
Zhang, X., Peng, W., Su, G., Su, S., Chen, J., 2018a. Thermionic energy conversion based on 3D Dirac semimetals. J. Phys. D Appl. Phys. 51, 405501.
Zhang, X., Ye, Z., Su, S., Chen, J., 2018b. Thermionic-thermoradiative converters. IEEE Electron. Device Lett. 39, 1429–1432.